

LARGE EDDY SIMULATIONS OF LOW-REYNOLDS NUMBER FLOWS IN THE COMPRESSIBLE REGIME

Pietro Catalano[1] & Francesco Antonio D'Aniello[1]

[1]C.I.R.A. - Italian Aerospace Research Center

Abstract

The focus of the paper is on the numerical simulations of flows at low Reynolds number at subsonic Mach numbers. The interest for the compressible aerodynamics of low-Reynolds number flow has recently grown for the possible use of aircraft for exploring the Martian surface. The reduced pressure and density of Mars atmosphere, together with the low temperatures, produce flight conditions characterized by very low Reynolds numbers, about 2% of those on the Earth, in combination with high Mach numbers, 1.5 times higher than the terrestrial ones. Large eddy simulations have been performed for the flow around the NACA 0012-34 airfoil at Reynolds number 1.1×10^4 and Mach numbers 0.20, 0.48, and 0.61. RANS simulations by in-house developed and an open-source code have been also carried out. The achieved results are compared to reference data available in literature. The focus is on the role of the Mach number and in particular on the behaviour of the lift coefficients that do not follow the classical compressibility rules.

Keywords: Low Reynolds number, Compressibility, Laminar Separation bubbles

1. Introduction

NASA and JAXA agencies are considering the airplanes as a feasible mean for exploring the Mars surface. In fact airplanes avoiding the morphology of the surface should obtain information wider and more detailed with respect to the ground rovers used in the past missions to Mars. The Mars

Table 1 – Comparison of environment between and Mars and Earth from [1]

		Mars	Earth
Acceleration of gravity	(m/s^2)	3.66	9.81
Atmospheric Pressure	(kPa)	$0.6 \approx 1$	101.3
Atmospheric Density	(Kg/m^3)	0.167	1.225
Coefficient of viscosity	(Kg/ms)	1.289×10^{-5}	1.789×10^{-5}
Gas constant	(J/KgK)	192	287
Ratio of specific heat	(-)	1.29	1.4
Speed of sound	(m/s)	228	340

atmosphere is 95% constituted by CO_2 and the force of gravity is about $1/3$ than the Earth's one. Mars airplane are expected to perform a flight at low Reynolds number in the range of $10^4 - 10^5$. At these Reynolds numbers, laminar separation bubbles often occur. The flow cannot sustain strong adverse pressure gradients and separates in the laminar regime and the transition takes place inside the separated shear layer. The velocity should be relatively high to produce enough lift and to ensure a stable flight in gusty atmosphere. The flight Mach number should range between 0.4 and 0.7.

The aim of the paper is to evaluate the dependence of the aerodynamic coefficients on Mach number. This effect has been scarcely investigated in literature because in the Earth atmosphere flows at low Reynolds numbers occur in the incompressible regime. The interest for compressible aerodynamics at low Reynolds number has turned out to be important when the use of aircraft for the exploring the Mars surface has been taken into consideration.

This study has been performed for the NACA 0012-34 airfoil because data at different Mach numbers are available in literature. This airfoil has been tested by experiments performed at University of Tohoku [2]. Catalano and D'Aniello [3] have performed RANS simulations by applying the SST $\kappa - \omega - \gamma - Re_\theta$ turbulence model by using the Ansys Fluent© software. It has been necessary applying levels of free-stream turbulence levels far higher than the ones usually employed to achieve reasonable results. Both numerical and experimental results have shown that the classical rules to take into account the compressibility effect do not hold at low-Reynolds number.

The aim of the present paper is to investigate the effect of the Mach number on low-Reynolds number flows by applying large eddy simulations. The fidelity CharLES software has been applied at Reynolds number 1.1×10^4 and Mach numbers 0.20, 0.48, and 0.61. Different incidences have been considered. RANS simulations have been also performed in order to make a more detailed analysis of numerical methods and models. The development of the turbulent structures and their influence on the separation regions and on the laminar bubbles are supposed to be the culprit of the behaviour of the aerodynamic coefficients with the Mach number.

2. Numerical Methods

The numerical simulation of the flow around the NACA0012-34 at low Reynolds number in the compressible regime is the subject airfoil of this paper. The main aim is to understand and explain the behaviour of the lift coefficient with the Mach number in the high viscous regime. The geometry of the airfoil is presented in figure 1. The NACA0012-34 airfoil is more thin in the front part and more thick in the rear part with respect to the classical NACA 0012.

The results presented and discussed in this paper have been achieved by applying the RANS in-house developed UZEN and the open-source SU2 codes and the Fidelity CharLES suite to perform large eddy simulations. The NACA0012-34 airfoil has been investigated experimentally at the Tohoku University and experimental data are available in literature [2].



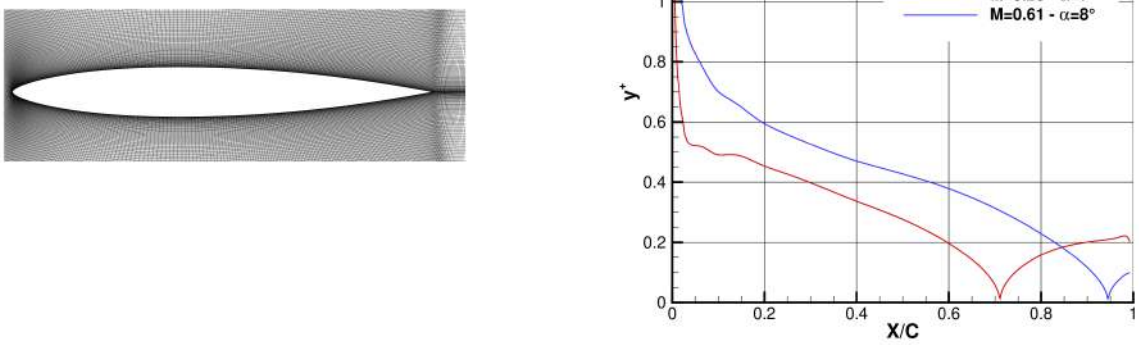
Figure 1 – Geometry of the NACA 0012-34

2.1 UZEN code

The CIRA in-house code UZEN (**U**nsteady **Z**onal **E**uler **N**avier Stokes) solves the compressible RANS equations on structured multi-block domains. The adopted spatial discretization consists of a central finite-volume formulation with explicit blended 2^{nd} and 4^{th} order artificial dissipation. The dual-time stepping technique is employed for time-accurate simulations [4]. The pseudo-time integration is carried out by an explicit hybrid multistage Runge-Kutta scheme. Classical convergence acceleration techniques, such as local time stepping and implicit residual smoothing, are available together with multigrid algorithm. Turbulence is modelled by either algebraic or transport equation models [5, 6]

and also hybrid RANS-LES methods are available [7]. UZEN is typically used for simulating steady and unsteady flows around complex aeronautical configurations[8]. Some peculiar phenomena [9] and particular devices [10, 11] can be reproduced.

A C-topology single-block computational grid with 1600 cells (1200 on body and $(200+200)$ on the wake) in the stream-wise and 200 cells in the wall-normal direction has been employed. A sketch of the grid with the resulting height of the first cell in viscous coordinates at different Mach numbers is shown in figure 2. The SST $\kappa-\omega-\gamma$ turbulence model [12] has been employed in the numerical simulations



(a) Grid around the airfoil

(b) y^+

Figure 2 – RANS grid and height of first cell in viscous coordinate y^+

2.2 SU2 code

The open-source CFD flow solver SU2 (formerly Stanford University Unstructured [13]) employs a vertex-based finite-volume formulation on general unstructured grids and operates on dual meshes through an edge-based data structure.
SU2 provides both a compressible and an incompressible solver. In the compressible solver, the convective fluxes in the governing equations are discretised using either central schemes, such as the well-known Jameson–Schmidt–Turkel (JST) scheme [14], or upwind formulations, like the basic Roe scheme and the Advection Upstream Splitting Method (AUSM) [15], including its low-dissipation variants. The incompressible solver, instead, features only the JST scheme and the Lax-Friedrichs scheme [16] at present. For temporal discretisation in unsteady problems, the code uses an implicit scheme combined with a dual-time-stepping strategy that ensures second-order accuracy in time.
The grid (figure 2) employed for UZEN code has been translated in unstructured format and used also for the simulations performed by SU2 solver. The $\gamma-\Re_\theta$ Langtry-Menter transition model [17] coupled with the Spalart-Allmaras model with the default Malan correlation has been used.

2.3 Fidelity CharLES

Fidelity CharLES is a collection of large-eddy-simulation flow solvers encompassing a variety of equation of state and physics-based modelling.

The flow solver CharLES is a massively parallel, finite volume, compressible flow solver. It utilizes a low dissipation spatial discretion based on principles of discrete entropy preservation where the

fluxes are constructed to globally conserve entropy in an inviscid, shock-free flow and conserve kinetic energy in an inviscid, low Mach number regime. The numerical scheme has been shown to be suitable for coarsely resolved large eddy simulations of turbulent flows that are especially sensitive to numerical dissipation. Time advancement is performed using a three-stage explicit Runge–Kutta scheme and the spatial discretization is formally second-order accurate. The code has been extensively validated, as shown in some recent applications [18, 19].

The Vreman model with constant model coefficient [20] is chosen as the subgrid-scale stress model to take into account the effect of the small dissipative scale on the resolved large scale.

The compressible version has been run by applying the MPI paradigm on X2135 GPU blades based on NVIDIA Ampere A100-64 accelerators of the Leonardo supercomputer of the EuroHPC Joint Undertaking (JU), hosted by the Italian CINECA consortium.

Unstructured grids based on Voronoi diagrams have been employed by applying the gridding module (Stitch), native to the CharLES solver suite. Isotropic hexagonal close-packed (HCP) cells are generated by computing the Voronoi diagram associated with a staggered point seeding in the domain. The Voronoi diagram associated with a given point seeding is unique once the seed points are defined. Each control volume contains the locus of space that is closer to that seed point than to any other seed point. Lloyd's algorithm is used to move the Voronoi seed points towards the cell centroid of each control volume, which improves the accuracy of the spatial flux calculations [21]. The grid is body-fitted and has regions of targeted refinement near viscous boundaries. The use of Voronoi diagram-based meshes allows for the rapid generation of high-quality grids with some guaranteed properties (for instance, the vector between two adjacent Voronoi sites is parallel to the normal of the face that they share). The computational grid, obtained by applying the Stitch mesh generator based on 3D clipped Voronoi diagrams, has about 29 million nodes and is shown in figure 3.

The height of first grid cell has been set in order to have a y^+ of order of magnitude of tens and an algebraic wall model boundary condition has been applied at the airfoil surfaces. At outflow a non-reflecting boundary condition with an imposed reference pressure has been applied, while the inflow density and velocity are imposed. Periodic boundary conditions are used at the side boundaries of the domain that extends 30 airfoil chord upstream and downstream and 0.1 chord in the span-wise direction. The Vreman sub-grid scale model has been used to account for the effects of the unresolved scales on the resolved ones.

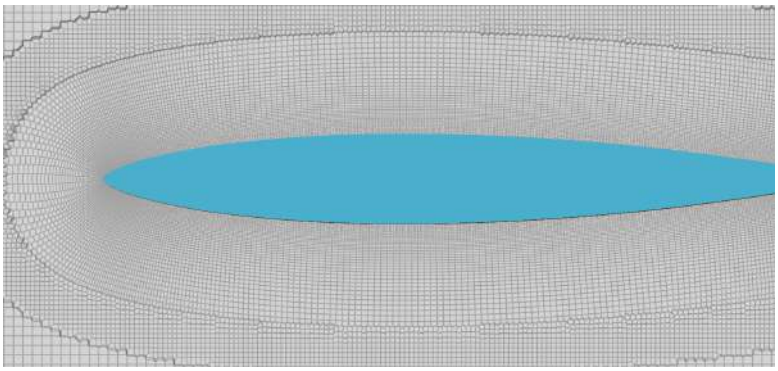


Figure 3 – Grid around the airfoil

3. Results and Discussion

The UZEN, SU2, and CharLES flow solvers have been applied to simulate the flow around the NACA 0012-34 airfoil at Reynolds number 1.1×10^4 and Mach numbers $0, 20$, 0.48, and 0.61.
The reference values of the Mars atmosphere have been used in the numerical simulations. The

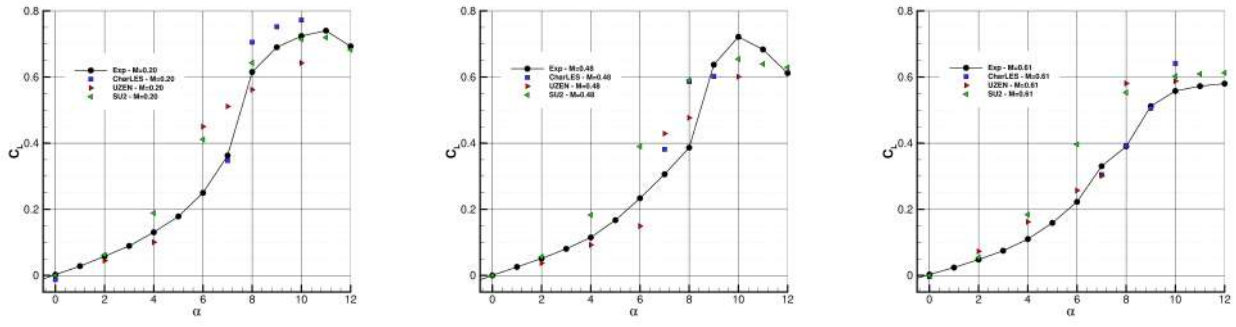
large eddy simulations by CharLES flow solver have been advanced in time for about 2000 through-flow-times (tft) and time-averaged for the last 1000 tft. The RANS simulations by the UZEN code have been performed by using the Jameson scheme with scalar artificial dissipation and applying the SST $\kappa - \omega - \gamma$ turbulence model [12] with values of free-stream turbulence increasing with incidence and Mach number. The RANS simulations by the SU2 code have been performed by using the Jameson scheme with matrix artificial dissipation and applying the Spalart-Allmaras turbulence model coupled with two transport equations for γ and $\Re_\theta$ [17].

3.1 Aerodynamic Coefficients

The lift coefficients achieved by RANS simulations and CharLES, in a limited number of α, are compared to the experimental data [2] in figure 4 and present very interesting characteristics. The RANS results by UZEN follow well the experimental data only at low-medium incidences. The C_L achieved by SU2 presents an acceptable agreement also at high incidence that generally gets worse as the Mach number increases. A global satisfactory agreement can be observed for the CharLES results with some discrepancies at the high incidence when the flow is approaching the stall. The non-linearity of the curve, likely due to the presence of bubbles, is somehow predicted better by the large eddy simulations.
A decrease of the C_L with the Mach number (at same α) is present in both numerical and experimental data and becomes very evident as α increases. This behaviour seems to be connected to the strong non-linearity presented by the lift curve and therefore connected to the Reynolds number and to the development of laminar separation bubbles on the airfoil surface.

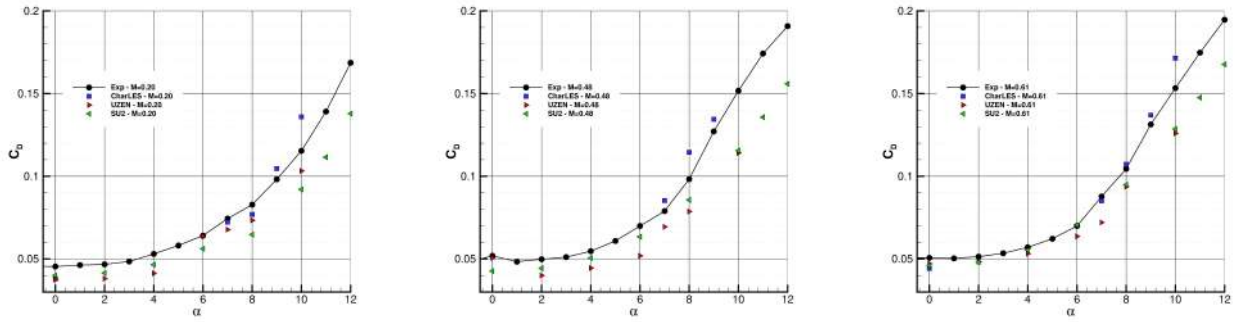
The drag coefficient is shown in figure 5. The RANS results always underestimate the experimental data with again better results provided by SU2. The CharLES C_D well follow the experimental curves at all the three Mach numbers and the agreement with the experiments becomes better at the same α at increasing Mach. It is worth noting that, with difference to C_L, the drag coefficient increases with the Mach number.

Finally, the drag polars of the airfoil are presented in figure 6. The decrease of the lift coefficients with the Mach number is quite evident by comparing the three plots of figure 6. The results by CharLES show an agreement with the experimental data definitely better than RANS data especially at Mach number 0.61. It seems that the RANS models return a separated flow but the production of turbulence is not enough for the reattachment. A scale-resolving method is needed to provide a qualitative correct formation of the turbulence structures.



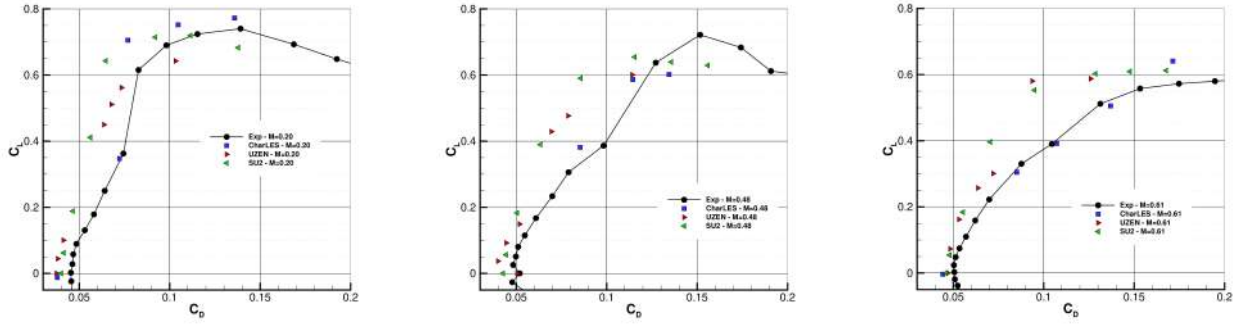
(a) M=0.20 (b) M=0.48 (c) M=0.61

Figure 4 – NACA0012-34 airfoil at $Re = 1.1 \times 10^4$: Lift Coefficient



(a) M=0.20 (b) M=0.48 (c) M=0.61

Figure 5 – NACA0012-34 airfoil at $Re = 1.1 \times 10^4$: Drag Coefficient



(a) M=0.20 (b) M=0.48 (c) M=0.61

Figure 6 – NACA0012-34 airfoil at $Re = 1.1 \times 10^4$: Drag Polar

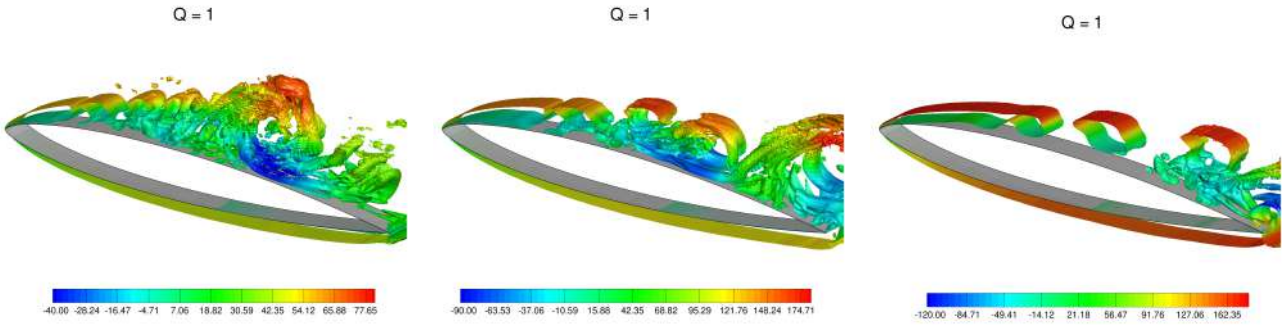
3.2 Flow fields

A description of the flow fields developing at Reynolds 1.1×10^4 at different Mach numbers around the airfoil can be found in Anyoji *et al.* [2]. The flow stands in the laminar regime and separates very close to the trailing edge already at $\alpha = 0^\circ$ at all the three Mach numbers taken into consideration. Then the separation point moves upstream as the incidence increases and a transition takes place starting from the lowest Mach number. The transition point, as well as the separation point, moves upstream with α and a laminar separation bubble then appears on the upper surface of the airfoil at both Mach numbers 0.20 and 0.48. The separation, transition and reattachment points move downstream with the Mach number and at the stall the flow is completely separated. It is worth noting that at Mach number 0.61, the flow is reported to undergo the transition to turbulence but no bubble is formed.
These characteristics can be retrieved also from the large eddy simulations. The development of the turbulence on the airfoil, as achieved by the CharLES flow solver, is reported at $\alpha = 9^\circ$ at the three Mach numbers in figure 7 by the Q-criterion i.e. the zone of the flow field where

$$\underline{\underline{Q}} = \frac{1}{2}\left[\| \underline{\underline{\Omega}} \|^2 - \| \underline{\underline{S}} \|^2 \right] = -\frac{1}{2}\frac{\partial u_i}{\partial x_j}\frac{\partial u_j}{\partial x_i} > 0 \tag{1}$$

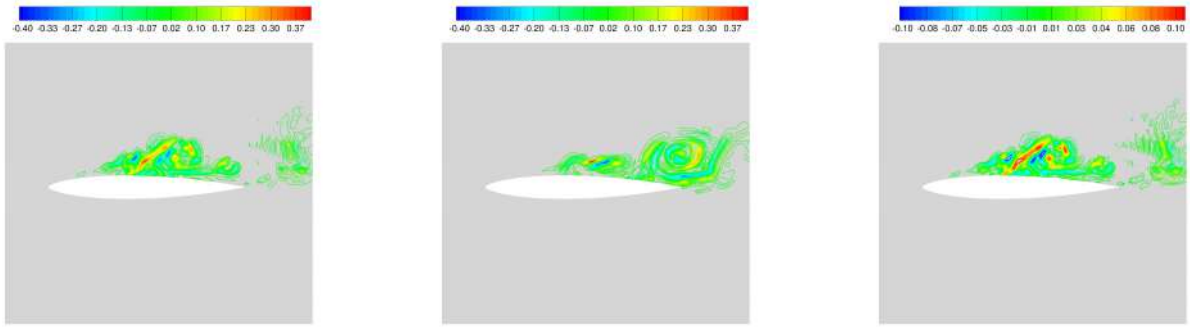
In particular, figure 7 shows the instantaneous isosurface $Q/(\frac{U_\infty}{C})^2 = 1$ coloured by the stream-wise velocity. The regions of separated flow can be identified. All the three plots show 2D structured that tend to break in turbulence by a Kelvin-Helmholtz instability. The transition moves downstream as the Mach numbers increases. At Mach number 0.20, the separation point is quite advanced in the front zone of the airfoil where the flow stands in laminar regime. The turbulence then develops in the separated region leading to the reattachment. A laminar separation bubble is obtained in the simulation. A similar situation occurs also at M=0.48 but with the transition taking place more downstream. On the contrary at Mach=0.61, the flow is laminar and separated up to almost the trailing edge. The

instantaneous span-wise velocity divided by the free-stream velocity $\frac{W}{U_\infty}$ is shown in figure 8. The flow becomes three-dimensional and potentially turbulent more downstream as the Mach number increases. The value of the three-dimensionality of the flow decreases with the Mach number and results much smaller at Mach=0.61 than at Mach=0.20 The numerical results by the large eddy simulations show that the increase of the Mach number delays the transition evidently making the flow more stable. The increased turbulence developing at low Mach numbers promotes the reattachment of the flow and the formation of laminar bubbles. The lift coefficient, as a consequence, results higher at the low Mach numbers.



(a) M=0.20 (b) M=0.48 (c) M=0.61

Figure 7 – NACA0012-34 airfoil at $Re = 1.1 \times 10^4$: Isosurface of Q coloured by the streammwise velocity at $\alpha = 9^\circ$



(a) M=0.20 (b) M=0.48 (c) M=0.61

Figure 8 – NACA0012-34 airfoil at $Re = 1.1 \times 10^4$: Field of $\frac{W}{U_\infty}$ at $\alpha = 9^\circ$

3.3 Pressure Coefficients

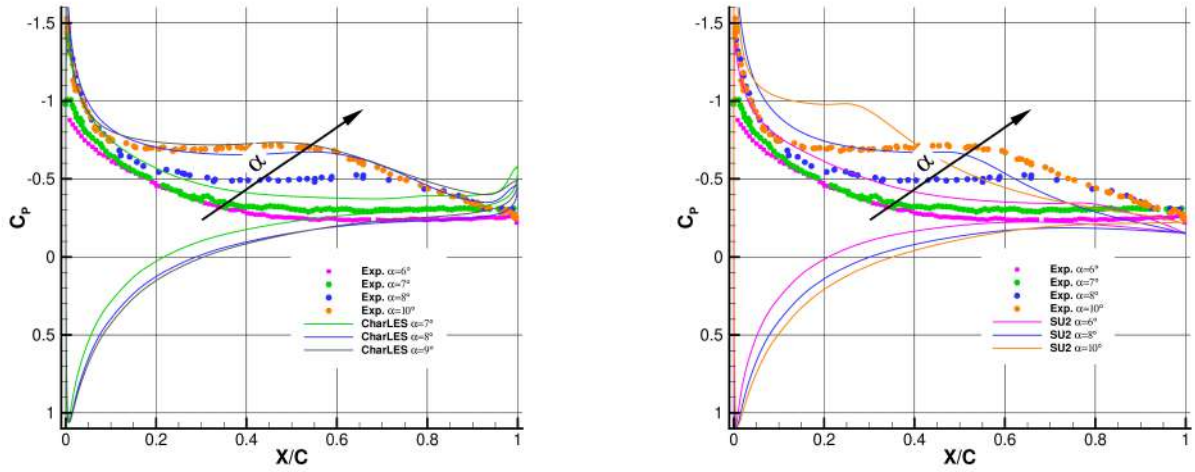
The same behaviour of the flow can be retrieved in the experimental pressure coefficients reported in figures 9 and 10 together with the C_P achieved by applying the CharLES suite and SU2 flow solvers at Mach number 0.48 and 0.61 respectively.

A systematic over-prediction of the experimental data can be noted in the CharLES results. At Mach 0.48, a very clear bubble is present in the experimental pressure distribution at $\alpha = 10^\circ$, but also at $\alpha = 8^\circ$ a pressure recovery is present in the C_P. A good qualitative agreement can be seen for the results achieved by CharLES. The large eddy simulations presents the classical distribution of a laminar bubble at both $\alpha = 8^\circ$ and 9°. It is worth noting the very good agreement between the CharLES results at $\alpha = 9^\circ$ with the experiments at $\alpha = 10^\circ$.

The C_P achieved by SU2 also show an over-prediction of the experimental data. A separation with a pressure recovery is present from $\alpha = 6^\circ$. The separation point moves upstream but the no re-

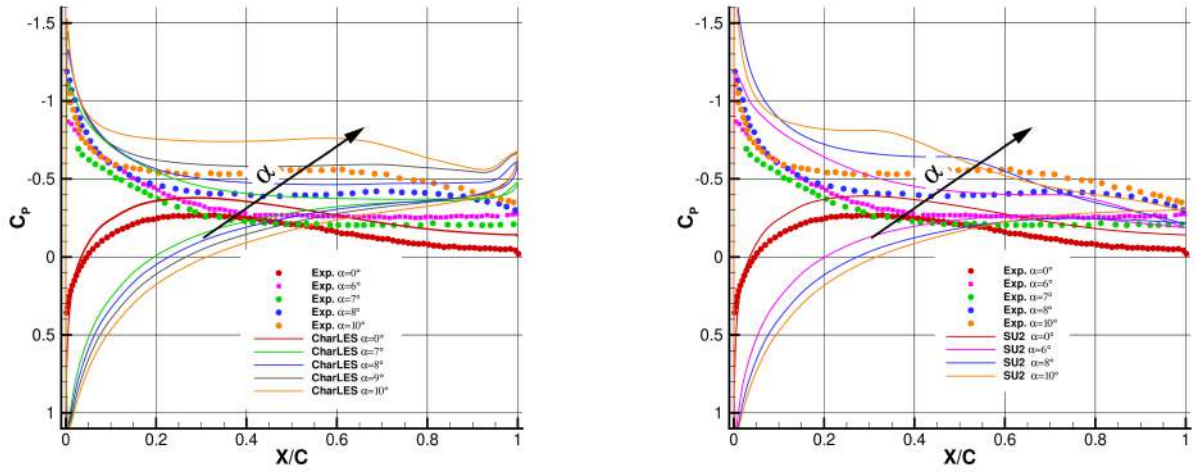
attachment is visible in the results.

At Mach 0.61, the experimental data present a weak pressure recovery at $\alpha = 8°$ and $10°$. The pressure recovery in SU2 C_P is visible from $\alpha = 6°$ while CharLES results have a recovery only at $\alpha = 10°$. It is worth noting that the numerical pressure distributions by CharLES show the track of a vortical structure in the trailing-edge zone at all the α but $\alpha = 0°$.
The qualitative characteristics of the flow field is globally predicted by the large eddy simulation better than the two RANS approaches with the method employed by SU2 providing better results.



(a) CharLES (b) SU2

Figure 9 – NACA0012-34 airfoil at $Re = 1.1 \times 10^4$ and $M = 0.48$: Pressure Coefficients. Solid lines: Numerical; symbols: Experimental [2]



(a) CharLES (b) SU2

Figure 10 – NACA0012-34 airfoil at $Re = 1.1 \times 10^4$ and $M = 0.61$: Pressure Coefficients. Solid lines: Numerical; symbols: Experimental [2]

4. Concluding Remarks

The flow around the NACA0012-34 airfoil has been analysed at Reynolds number 1.1×10^4 by RANS and large eddy simulations. Three Mach numbers up to high subsonic regime have been considered. The compressible regime at low Reynolds number would be typical of machines flying in the Martian low atmosphere for exploring the surface of the planet.

The present large eddy simulations have shown to well predict the qualitative flow characteristics. The strong non-linearity of the lift coefficient has been reproduced and the agreement for drag polar of the airfoil is quite good especially at Mach 0.61. The RANS approach has been applied with turbulence models that make use of transition functions but the results have been satisfactory only at low-medium incidences in the linear zone of the lift coefficient. The use of the two transport equations transition model (coupled with the Spalart-Almaras turbulence model) implemented in SU2, allowed to qualitatively reproduce experimental data showing all the main characteristics of the aerodynamic coefficients but with less accuracy with respect to the large eddy simulations.

An interesting aspect, already highlighted in literature, is the decrease of the lift coefficient with the Mach number. The large eddy simulations performed around the NACA0012-34 airfoil have shown that the behaviour of the C_L with the Mach number is, as expected, essentially due to the low Reynolds number and to the development of the turbulence that leads to the formation of laminar bubbles. At low Reynolds number, the flow stands in laminar regime and tends to separate because is not able to withstand the adverse pressure gradients. Turbulence develops first at the lowest Mach number investigated (0.20) leading to a re-attachment of the flow while the laminar regime is kept almost up to the stall at the highest Mach number considered (0.61). This causes a strong non-linearity in the lift curve which results to be much more pronounced at low Mach number making the C_L greater at Mach 0.20 than at Mach 0.61. This aspect of the flow has been reproduced only by large eddy simulations. The RANS models have provided a separated flow that does not become enough turbulent for a reattachment. It seems that a scale-resolving method is needed to return a qualitative correct development of the turbulent structures that lead to the formation of a laminar bubble. The increase of the Mach number has a weak effect at low incidence but delays the transition to turbulence and the formation of the bubbles at high angles of attack.

It is worth noting that, instead, the drag coefficient remains increasing with the Mach number.

5. Contact Author Email Address

mailto: p.catalano@cira.it

6. Copyright Statement

The authors confirm that they, and/or their company or organization, hold copyright on all of the original material included in this paper. The authors also confirm that they have obtained permission, from the copyright holder of any third party material included in this paper, to publish it as part of their paper. The authors confirm that they give permission, or have obtained permission from the copyright holder of this paper, for the publication and distribution of this paper as part of the ICAS proceedings or as individual off-prints from the proceedings.

7. Acknowledgements

The authors wish to acknowledge the CINECA award under the ISCRA initiative, for the availability of high-performance computing resources and support

References

[1] W. J. F. Koning, W. Johnson, and H. F. Grip. Improved mars helicopter aerodynamic rotor model for comprehensive analyses. *AIAA JOURNAL*, 57(9):3969 – 3979, 2019.

[2] Anyoji; Numata; Nagai; Asai. Effects of mach number and specific heat ratio on low-reynolds-number airfoil flows. *AIAA Journal*, Vol. 53(No. 6), 2015.

[3] P. Catalano and F. A. A'Aniello. Numerical analysis of low-reynolds-number flows in earth and mars atmosphere. *Journal of Aircraft*, 62(5):1363 – 1375, 2025.

[4] C. Marongiu, P. Catalano, M. Amato, and G. Iaccarino. U-zen: A computational tool solving u-rans equations for industrial unsteady applications. $34^{th} AIAA Fluid Dynamics Conference and Exhibit, 2004$.

[5] P. Catalano and R. Tognaccini. Turbulence modeling for low-reynolds-number flows. *AIAA Journal*, 48(8):1673–1685, 2010.

[6] P. Catalano, B. Mele, and R. Tognaccini. On the implementation of a turbulence model for low reynolds number flows. *Computers and Fluids*, 109:67–71, 2015.

[7] P. Catalano. Application of a hybrid rans-les method to free shear layers. *ASME International Mechanical Engineering Congress and Exposition, Proceedings (IMECE)*, 7, 2019.

[8] P. Eliasson, P. Catalano, M.-C.L. Pape, J. Ortmann, E. Pelizzari, and J. Ponsin. Improved cfd predictions for high lift flows in the european project eurolift ii. *Collection of Technical Papers - AIAA Applied Aerodynamics Conference*, 3:1614–1631, 2007.

[9] G. Iaccarino, C. Marongiu, P. Catalano, and M. Amato. Rans modeling and simulations of synthetic jets. 2^{nd} *AIAA Flow Control Conference*, 2004. AIAA paper 2004-2223.

[10] P. Catalano, D. De Rosa, B. Mele, R. Tognaccini, and F. Moens. Performance improvements of a regional aircraft by riblets and natural laminar flow. *Journal of Aircraft*, 57(1):29–40, 2020.

[11] A. Marino, P. Catalano, C. Marongiu, P. Peschke, C. Hollenstein, and R. Donelli. Effect of high voltage pulsed dbd plasma on the aerodynamic performances in subsonic and transonic conditions. 43^{rd} *Fluid Dynamics Conference*, 2013.

[12] Florian R. Menter, Pavel E. Smirnov, Tao Liu, and Ravikanth Avancha. A one-equation local correlation-based transition model. *Flow, Turbulence and Combustion*, 95(4):583–619, 2015.

[13] Thomas D. Economon, Francisco Palacios, Sean R. Copeland, Trent W. Lukaczyk, and Juan J. Alonso. SU2: An Open-Source Suite for Multiphysics Simulation and Design. *AIAA Journal*, 54(3):828–846, 2016.

[14] Antony Jameson. Artificial Diffusion, Upwind Biasing, Limiters and Their Effect on Accuracy and Multigrid Convergence in Transonic and Hypersonic Flows. In *11th Computational Fluid Dynamics Conference*, page 3359, 1993.

[15] Meng-Sing Liou and Christopher J. Steffen. A New Flux Splitting Scheme. *Journal of Computational Physics*, 107(1):23–39, 1993.

[16] Kurt O. Friedrichs and Peter D. Lax. Systems of Conservation Equations With a Convex Extension. *Proceedings of the National Academy of Sciences*, 68(8):1686–1688, 1971.

[17] F.R. Menter, R.B. Langtry, S.R. Likki, Y.B. Suzen, P.G. Huang, and S. Volker. A correlation-based transition model using local variables - part 1: Model formulation. *J Turbomach*, 128(3):413–422, 2006.

[18] L. Fu, M. Karp, S. T. Bose, P. Moin, and J Urzay. Shock-induced heating and transition to turbulence in a hypersonic boundary layer. *Journal of Fluid Mechanics*, 909(A8), 2021.

[19] A Lozano-Duran, S. T. Bose, and P. Moin. Performance of wall-modeled les with boundary-layer-conforming grids for external aerodynamics. *AIAA Journal*, Vol. 60(No. 2):747 – 766, 2022.

[20] A. Vreman. An eddy-viscosity subgrid-scale model for turbulent shear flow: Algebraic theory and applications. *Phys. of Fluids*, 16:3670 – 3681, 2004.

[21] Q. Du, M. Emelianenko, and L. Ju. Convergence of the lloyd algorithm for computing centroidal voronoi tessellations. *SIAM journal on numerical analysis*, 44:102 – 119, 2006.